Geophysical Research Letters

Supporting Information for

Deep Short-term Slow Slip and Tremor in the Manawatu Region, New Zealand

Shannon L. Fasola[1], Noel M. Jackson[1], and Charles A. Williams[2]

[1]Department of Geology, University of Kansas, Lawrence, KS.

[2]GNS Science, Lower Hutt, New Zealand.

Contents of this file

Introduction

This Supporting Information includes details on the methods used and additional figures supporting the main text.

Text S1. Methods

GNSS Post-Processing

For this study we used daily time-series solutions from continuous GNSS stations from the GeoNet network on the North Island (GNS Science, 2000). GNSS data processing methods are outlined on the GeoNet website. We referenced GNSS time series to the fixed Australian plate using the plate model of Altamimi et al. (2012). Offsets due to antenna changes and earthquakes were estimated by differencing the average positions of 10 days before and after the offset and were then removed. Timing of the offsets were obtained from the University of Nevada-Reno steps database (http://geodesy.unr.edu/NGLStationPages/steps.txt). Outliers, any day for which there was more than a 4 mm difference in the horizontal position and/or

more than a 14 mm difference in the vertical position from a running mean with a window of 6 data points, were removed from all 3 components regardless of which criteria was met. There was a common mode signal on all stations in the network. Therefore, we regionally filtered the time series by averaging a select set of detrended time series with offsets removed from stations far from the Hikurangi Trench that have close to linear behavior. Regional stations used for averaging were AUCK, CORM, KTIA, WARK, WHNG (Figure S1). The averaged time series (i.e., the common mode signal) was then subtracted from the stations that exhibit tectonic deformation.

Determining Surface Velocity Uncertainties

The uncertainty of the inter-tremor velocities ($\sigma_{inter\text{-}tremor}$) for each of the three scenarios was determined by taking the standard deviation from a population of velocities generated through random resampling of the displacement increments. For each set, we randomly resampled the displacement increments without replacement 10,000 times, generated a cumulative displacement time series and performed a linear regression on the cumulative displacement time series to obtain a velocity for each iteration. We kept the duration of the displacement increment during resampling. Since the true tremor velocity was calculated by subtracting the inter-tremor velocity from the uncorrected tremor velocity, we similarly found the uncertainty of the uncorrected tremor velocity ($\sigma_{tremor\ before\ correction}$) through random resampling and then propagated uncertainties to determine the uncertainty of the true tremor velocity (σ_{tremor}):

$$\sigma_{tremor} = \sqrt{(\sigma_{\ tremor\ before\ correction})^2 + (\sigma_{\ inter-tremor})^2}$$

Robustness of Decompositions

In order to quantify the robustness of these decompositions with regard to background noise levels, we followed the modified bootstrapping approach of Rousset et al. (2019). Using the same number of tremor clusters as in the catalog, we randomly chose start times from the time series and randomly sampled the tremor durations without replacement to generate a synthetic catalog of tremor clusters to perform decompositions with. Periods of tremor from the real catalog were removed before running the decompositions with the synthetic tremor catalog. For decomposition of the SSE and inter-SSE times, we also removed periods of inter-SSE and SSE, respectively, to generate a synthetic 'SSE-only time series' and 'inter-SSE-only time series'. We performed these decompositions for 1) the entire time series, 2) during mid-to-long-term SSE time series, and 3) inter-SSE time series for the horizontal components 10,000 times and assumed that the decomposition was robust if the average velocity acquired for the real tremor periods was more than 2σ from the mean of velocities obtained with the random decompositions associated with noise or the inter-tremor periods. Rousset et al. (2019) used a 3σ threshold, but due to the likely incomplete tremor catalog, we lowered the threshold to 2σ. The decompositions for the entire time series were found to be robust for the east component of eight stations (Figure S7). The decompositions for the SSE time series were also found to be robust for the east component of eight stations (Figure S8). Fewer stations were found to be

robust for the north components, mainly because they are less sensitive to slip on the subduction interface. The random decompositions for the inter-SSE time series indicated a smaller difference between the real average velocity of tremor periods and the mean of the randomly generated velocities. For the east and north components no stations were greater than 2σ but 3 and 4 were greater than 1σ, respectively (Figure S9).

This modified bootstrapping technique as a method of testing the robustness of the decompositions is station specific. Therefore, we ran the decomposition on a select number of GNSS stations on the southern part of the North Island which was further from the Manawatu tremor, other regions of SSEs, and the Taupo volcanic zone to confirm that the tremor associated signal was confined to where tremor was observed (Figure 3b). To further support the validity of a geodetic signal only at stations nearest the tremor, we applied the modified bootstrapping technique to those far-field stations on which we ran the decompositions. As we expected, none of the east component time-averaged velocities of the far-field stations were found to be robust for decomposition of the entire time series, signifying the decomposition method of the Manawatu tremor did not detect a discernible geodetic signal at stations further from the tremor.

Calculation of Moment Rates

We calculated a total moment rate for each of the three modeled slip rate solutions. For each triangular patch, we found the time-averaged moment rate using the slip rate, area, and effective shear modulus for that patch and then summed the moment rates for the entire slip area. We consider both the variation of the shear modulus within the volume as well as possible 'jumps' in the shear modulus across the fault. To do this, we sample the properties on either side of the fault, assuming a distance of 100 m normal to the fault on each side, and then compute an effective shear modulus using the technique described by Wu and Chen (2003). We estimated the average moment per tremor burst by multiplying the moment rate for each slip patch by the average duration of tremor burst for that regime and totaling the moment (Table S1).

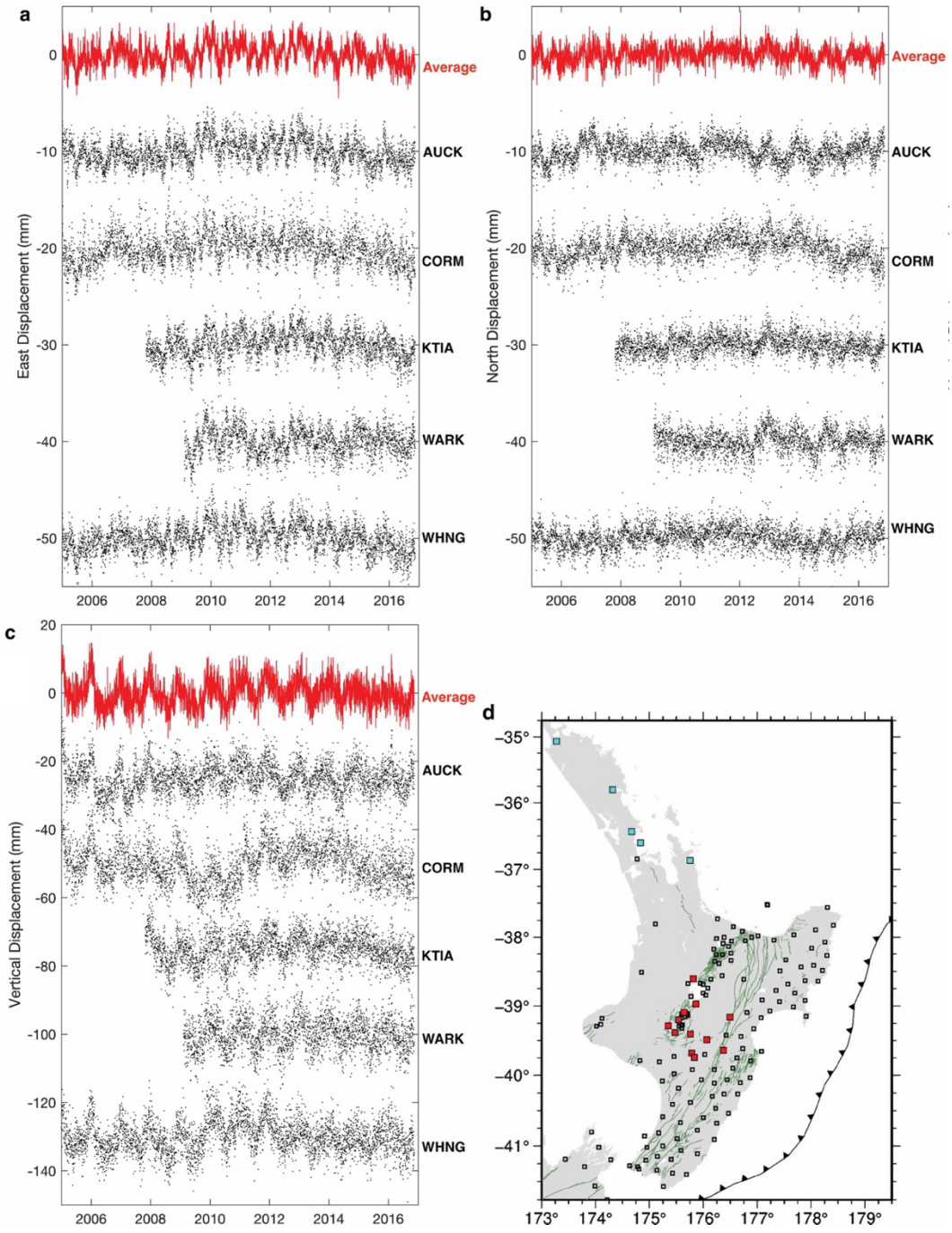

Figure S1. Time series of regional common mode signal. Black dots are detrended GNSS time series with offsets removed from stations far from the Hikurangi Trench that have close to linear behavior and were used in averaging to determine the common mode signal. Red line represents the average of those regional time series. a) East component. b) North component. c) Vertical component. d) Map of GeoNet GNSS stations (squares). Stations used for determining common mode signal and for decomposition are colored light blue and red, respectively.

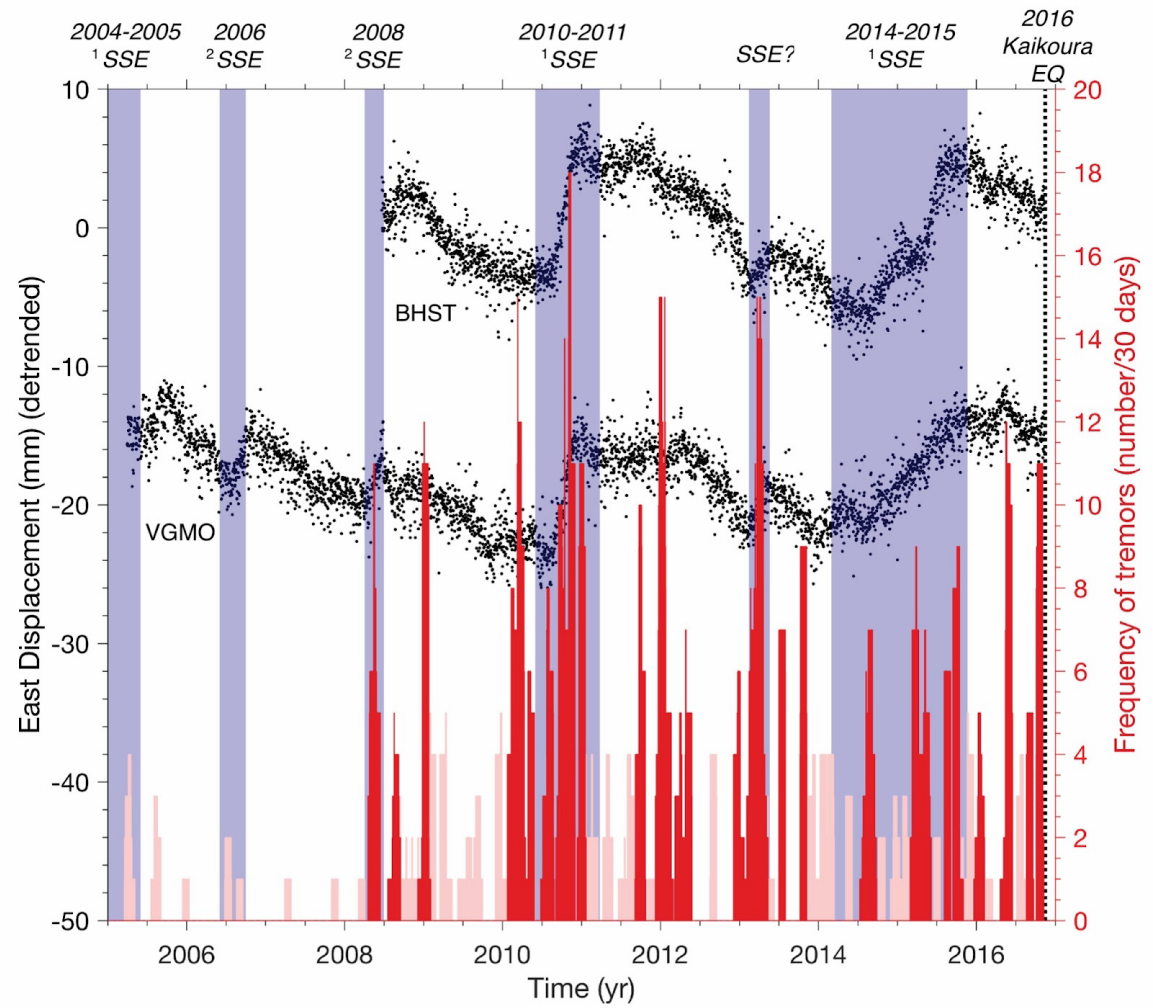

Figure S2. Tremor density and GNSS displacement plot. The tremor density (red and pink bars) is based on a 30-day moving window of the tremor catalog from Romanet and Ide (2019). Red bars are tremor that met the criteria to be in a cluster using a minimum of 5 events per cluster and a minimum inter-cluster duration of 22 days. The GNSS displacements consist of the detrended daily eastward displacements (black dots) at the BHST and VGMO GeoNet GNSS stations. Purple shaded areas represent timing of known deep mid- to long-term SSEs in the [1]Manawatu and [2]Kaimanawa regions, respectively. There may have been a deep SSE in 2013 similar to the 2006 and 2008 mid-term Kaimanawa SSEs (personal communication with Laura Wallace) which is also shaded purple. Black dotted line marks the time of the 2016 M_W 7.8 Kaikoura earthquake and the end of data analyzed in this study.

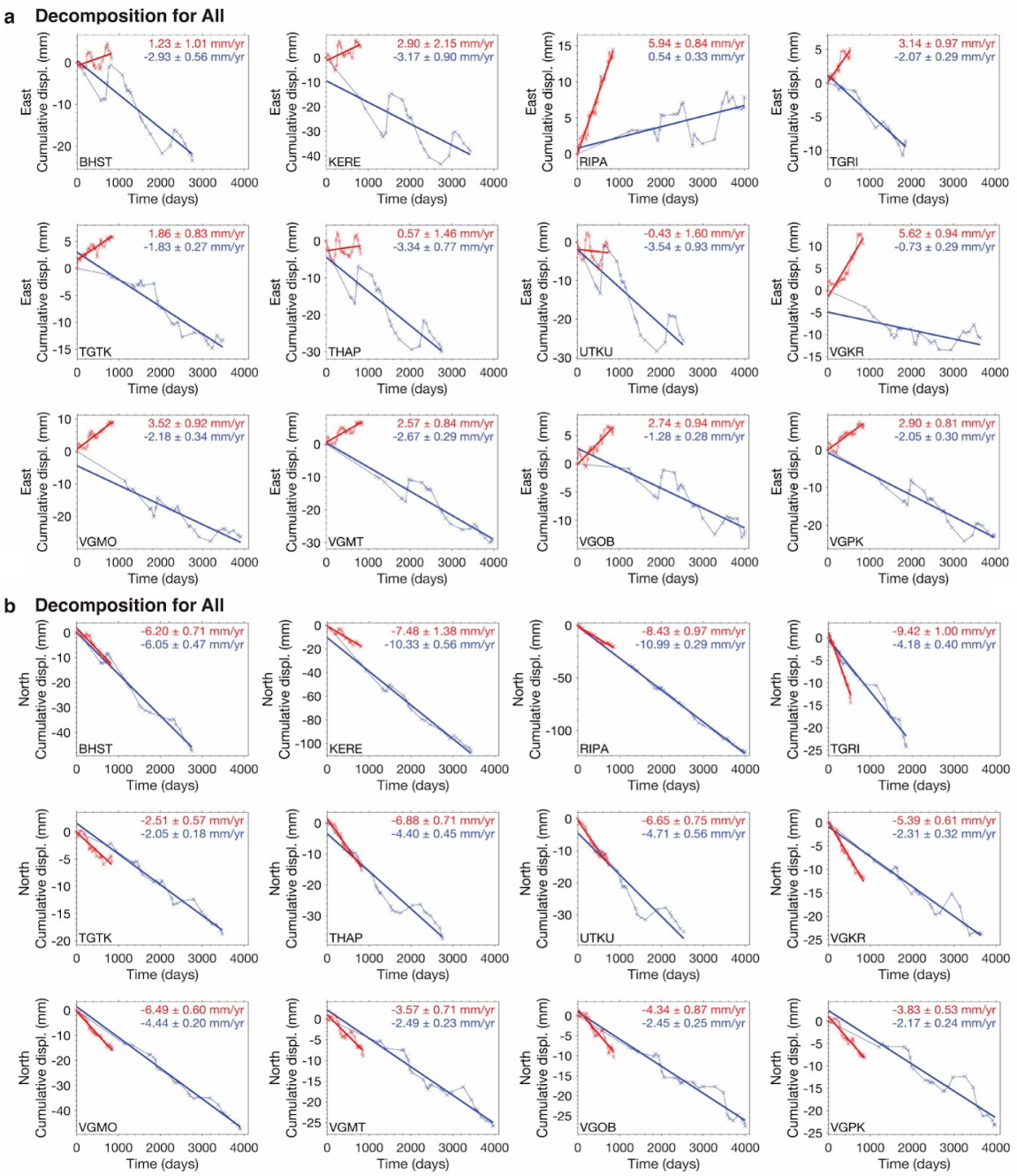

Figure S3. Decomposition of the entire time series a) east and b) north components from 2005 until the 2016 Kaikoura earthquake. Red and blue curves indicate cumulative offsets during tremor and inter-tremor periods, respectively. Values represent slope of the best fit line and 1σ uncertainty determined from random resampling of cumulative displacement increments.

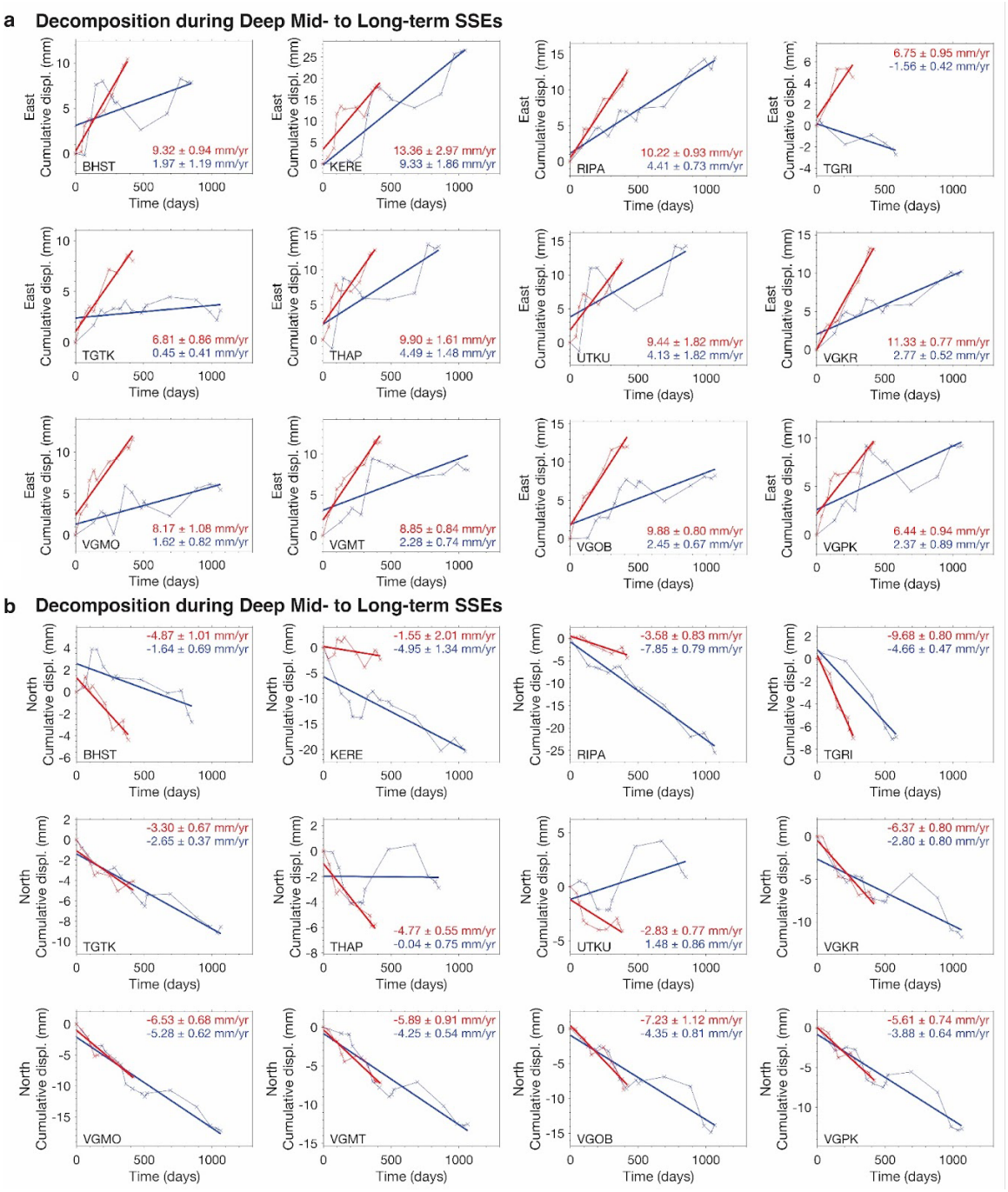

Figure S4. Decomposition of the GNSS time series a) east and b) north components during known deep 2004-2005, 2006, 2008, 2010-2011, 2013, and 2014-2015 slow slip events in the Manawatu and Kaimanawa regions. Red and blue curves indicate cumulative offsets during tremor and inter-tremor periods, respectively. Values represent slope of the best fit line and 1σ uncertainty determined from random resampling of cumulative displacement increments.

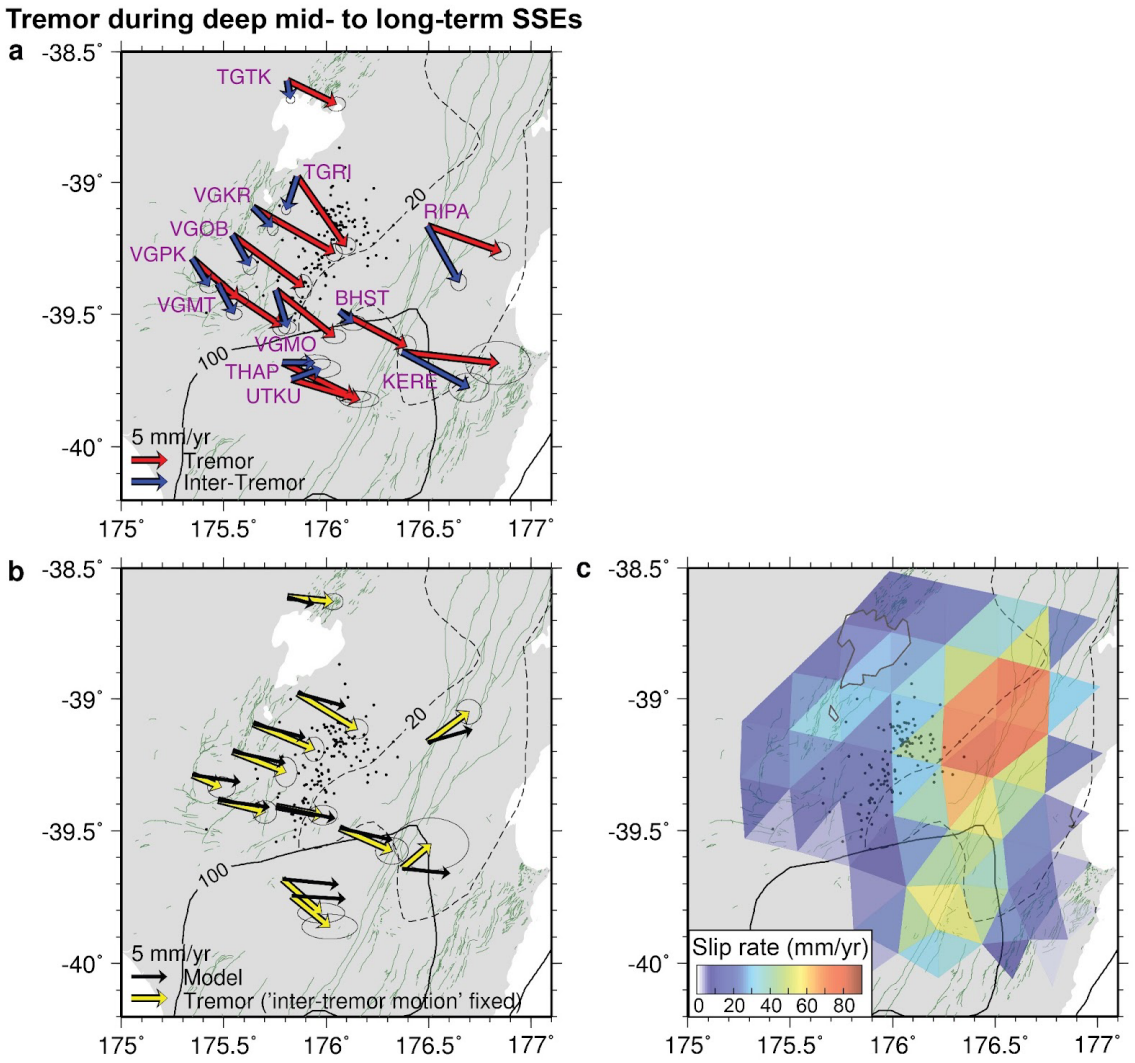

Figure S5. Time-averaged displacement rate and slip rate for tremor bursts during the mid- to long-term SSEs in Manawatu and Kaimanawa regions. a) Displacement rate of tremor (red arrows) and inter-tremor periods (blue arrows) with 1σ uncertainties are shown. b) Comparison of the true tremor displacement rates with the 'inter-tremor motion' fixed (yellow arrows) and 1σ uncertainty and modeled tremor displacement rates obtained from inversion (black arrows). c) Time-averaged slip rate during tremor bursts as estimated by static slip inversion.

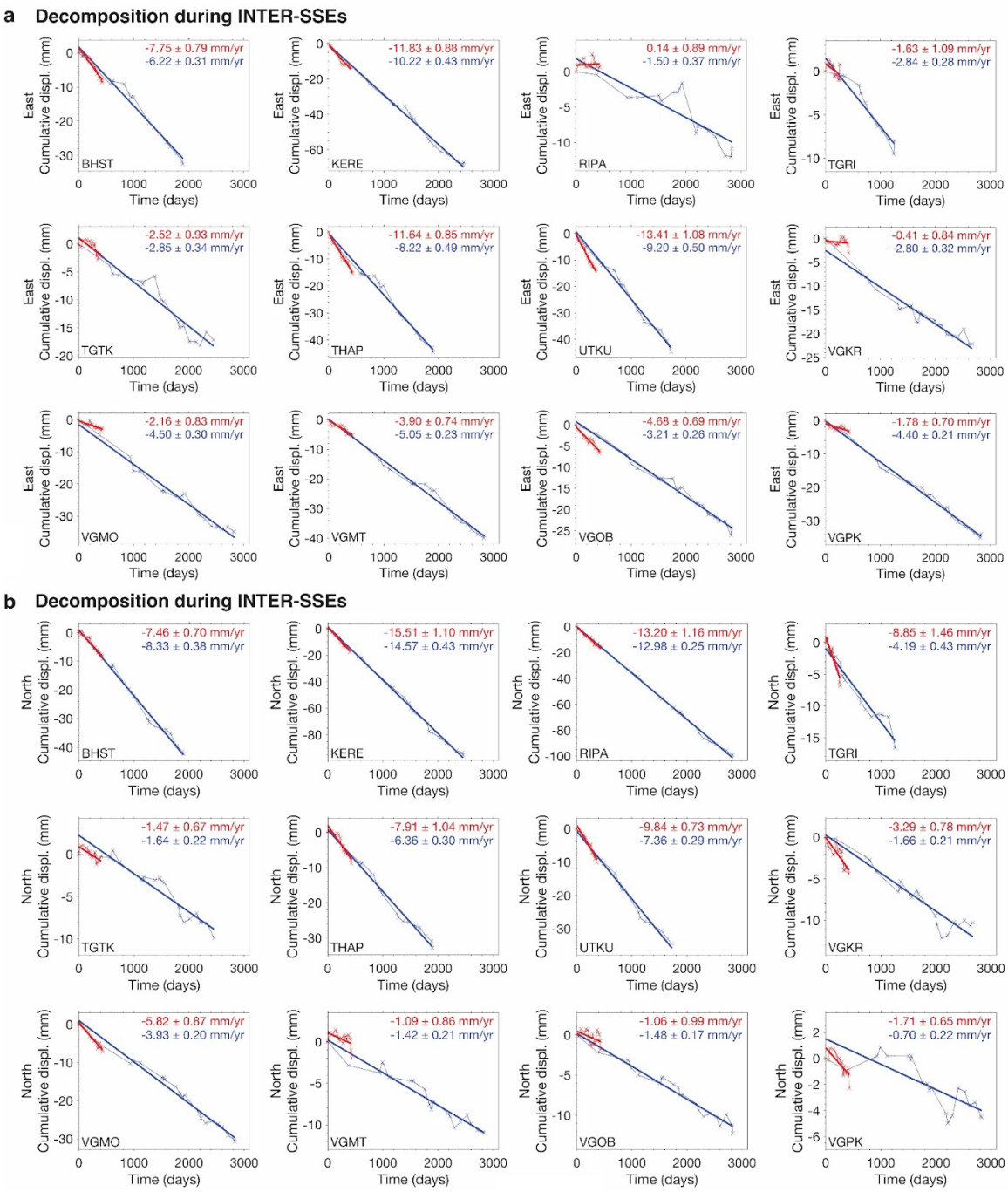

Figure S6. Decomposition of the GNSS time series. a) east and b) north components during inter-SSE time in the Manawatu and Kaimanawa regions: 2005 SSE to 2006 SSE, 2006 SSE to 2008 SSE, 2008 SSE to 2010-2011, 2010-2011 SSE to 2013 SSE, 2013 SSE to 2014-2015 SSE, and 2014-2015 to 2016 Kaikoura earthquake. The red and blue curves indicate the cumulative offsets during tremor and inter-tremor periods, respectively. Values represent slope of the best fit line and 1σ uncertainty determined from random resampling of cumulative displacement increments.

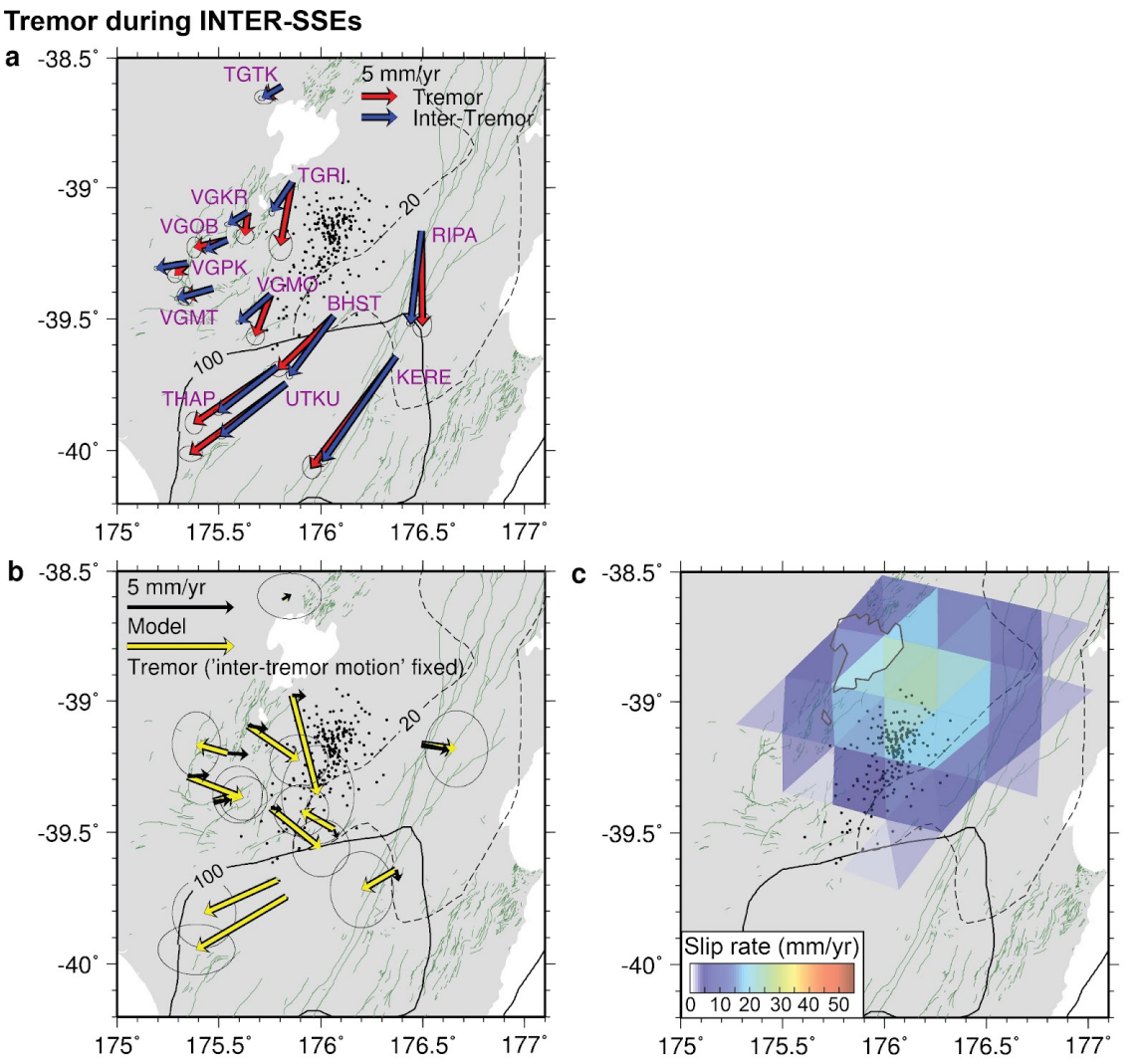

Figure S7. Time-averaged displacement rate and slip rate for tremor bursts during the inter-SSE periods. a) Displacement rate of tremor (red arrows) and inter-tremor periods (blue arrows) with 1σ uncertainties are shown. b) Comparison of the true tremor displacement rates with the 'inter-tremor motion' fixed (yellow arrows) and 1σ uncertainty and modeled tremor displacement rates obtained from inversion (black arrows). Due to the small values of the modeled vectors, we enlarged the 5 mm/yr scale. c) Time-averaged slip rate during tremor bursts as estimated by static slip inversion.

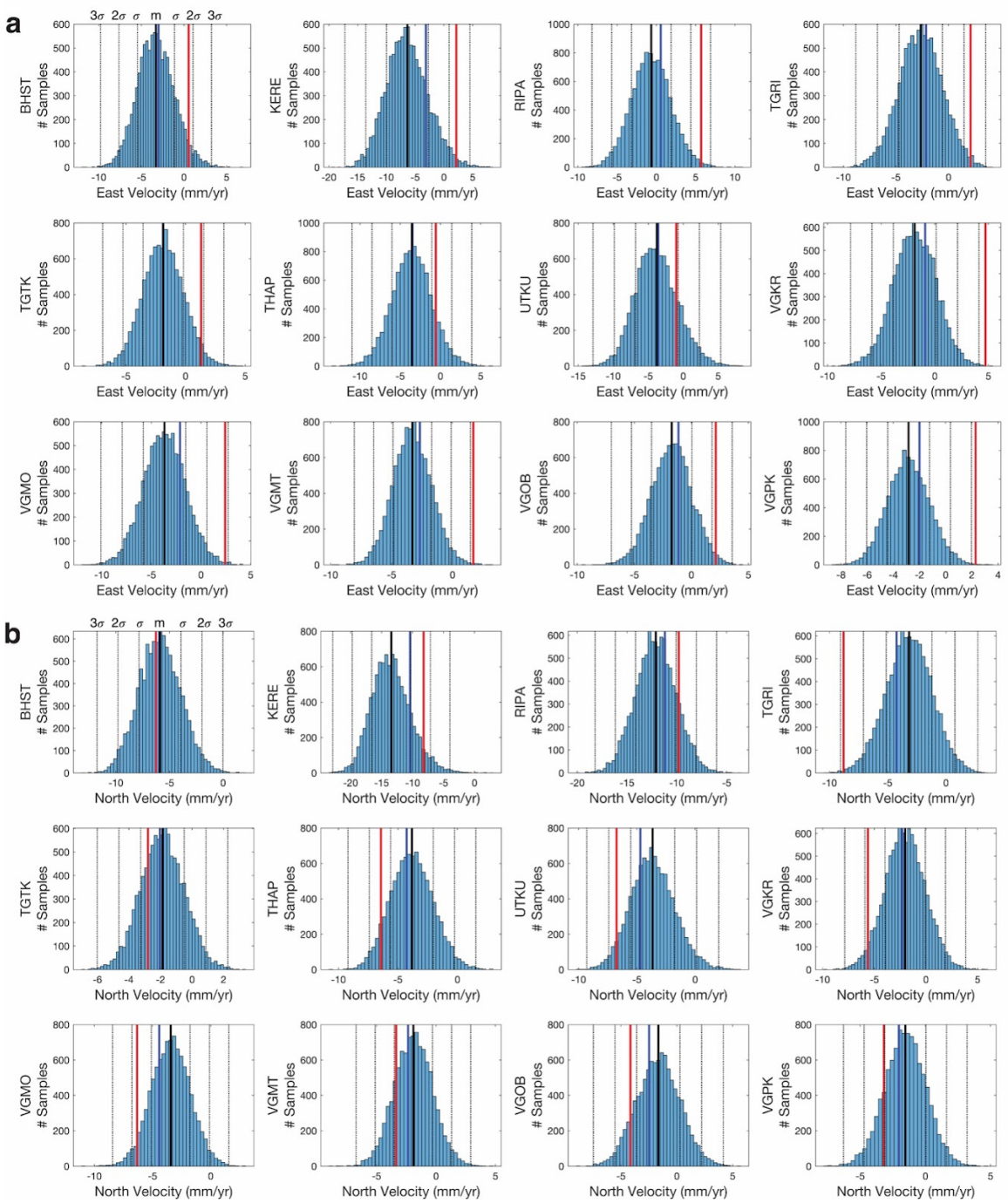

Figure S8. Histogram of velocities obtained by random decomposition of the entire time series with known tremor periods removed. For the decomposition, we randomly selected times of tremor clusters with the same number of clusters and durations as the real tremor catalog. The mean of the distribution is indicated by a solid black line whereas the σ, 2σ, and 3σ of the distribution are indicated by dashed lines. The red and blue lines indicate the averaged velocities obtained respectively for the tremor and inter-tremor periods. a) East velocity. b) North velocity.

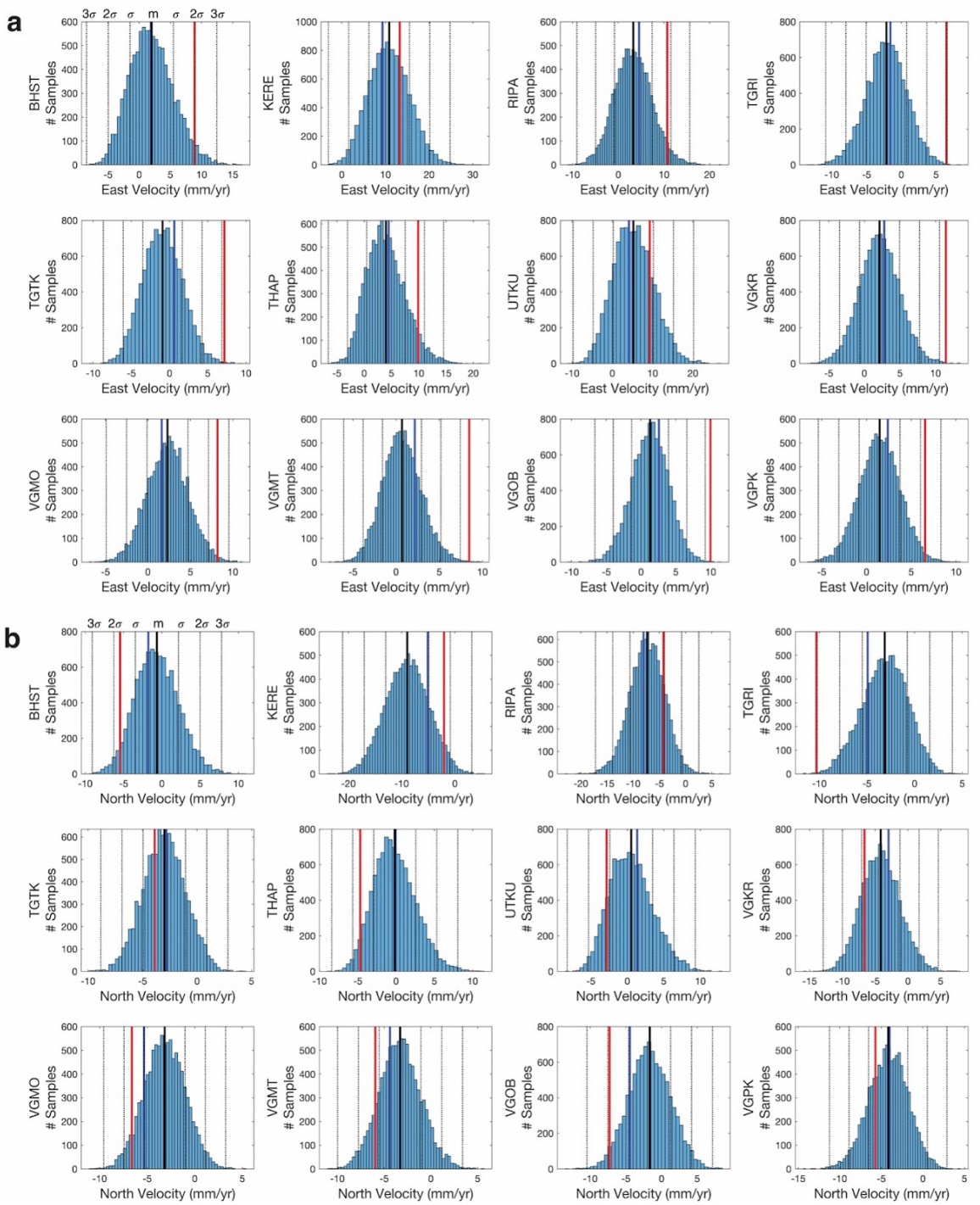

Figure S9. Histogram of velocities obtained by random decomposition of the time series of the deep mid- to long-term SSEs with known tremor periods removed. For the decomposition, we randomly selected times of tremor clusters with the same number of clusters and durations as that which occurs during the deep SSEs. The mean of the distribution is indicated by a solid black line whereas the σ, 2σ, and 3σ of the distribution are indicated by dashed lines. The red and blue lines indicate the averaged velocities obtained respectively for the tremor and inter-tremor periods. a) East velocity. b) North velocity.

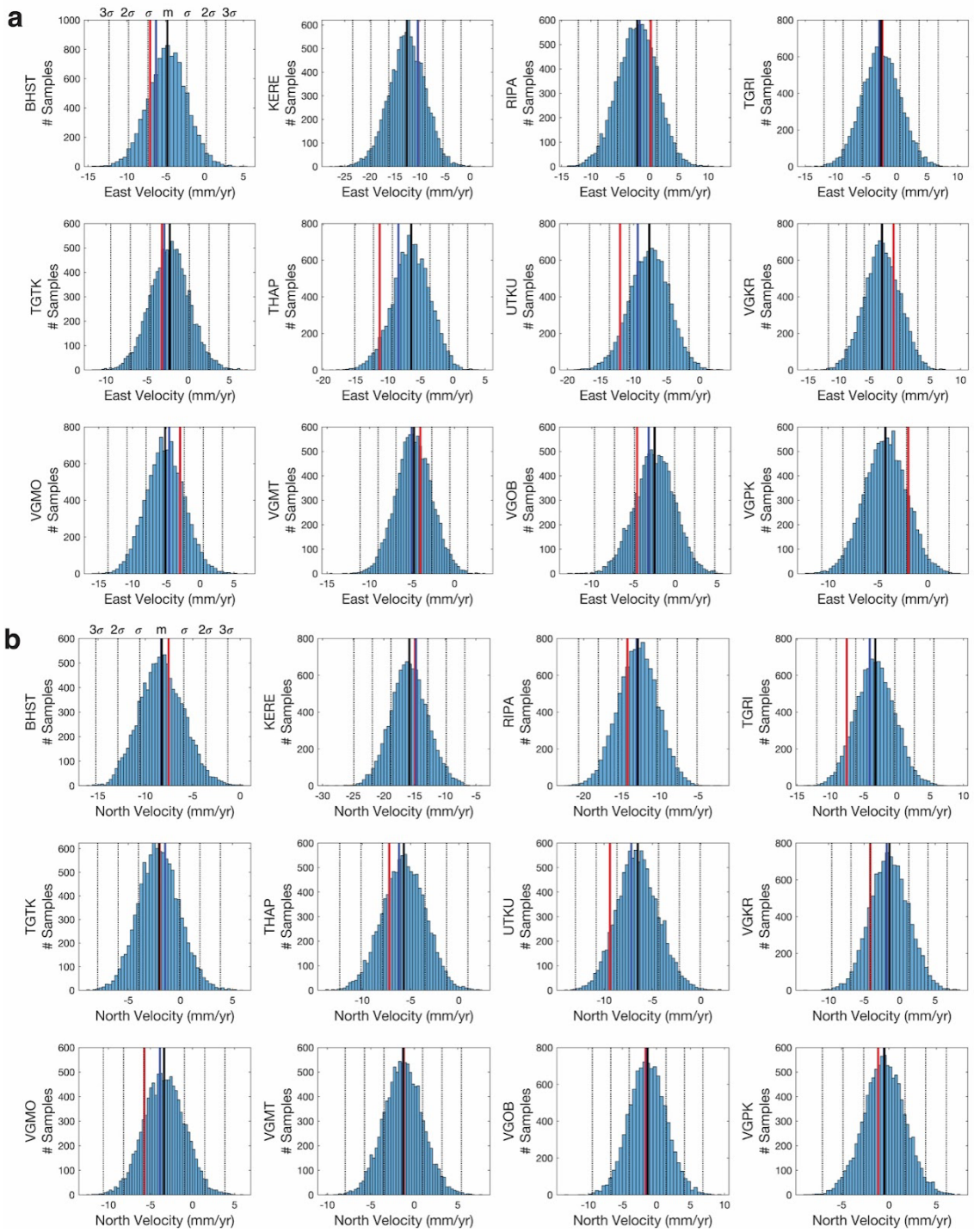

Figure S10. Histogram of velocities obtained by random decomposition of the time series of inter-SSEs with known tremor periods removed. For the decomposition, we randomly selected times of tremor clusters with the same number of clusters and durations as that which occurs during the inter-SSEs. The mean of the distribution is indicated by a solid black line whereas the σ, 2σ, and 3σ of the distribution are indicated by dashed lines. The red and blue lines indicate the averaged velocities obtained respectively for the tremor and inter-tremor periods. a) East velocity. b) North velocity.

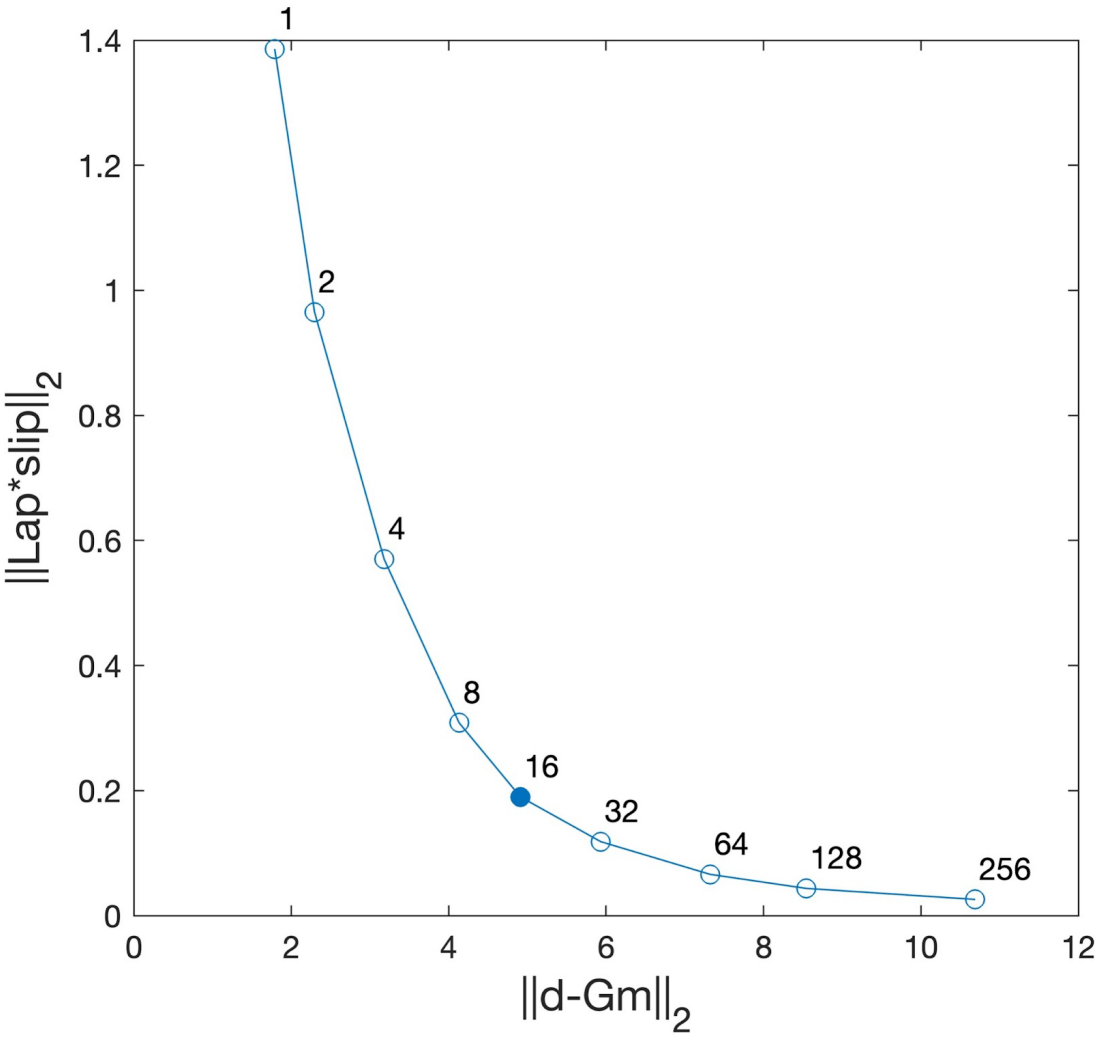

Figure S11. L-curve used to select the smoothing parameter γ where the y-axis is the 2-norm of the discrete Laplacian of the slip rate distribution and the x-axis is the 2-norm of the residuals. Numbers represent values of the smoothing parameter with 16 being the selected value.

Table S1. Summary of deep, ETS-like events in the Manawatu-Kaimanawa region detected through decomposition.

	Max Slip Rate (mm/yr)	Cumulative Moment Rate (Nm/yr)	Average Duration of Tremor Bursts (days)	Average Moment per Tremor Burst (Nm)	Average Equivalent M_w per Tremor Burst
All Tremor	51	2.4×10^{19}	23	1.5×10^{18}	5.0
Tremor during SSEs	80	3.4×10^{19}	32	3.0×10^{18}	5.2
Tremor during Inter-SSEs	25	9.4×10^{18}	17	4.4×10^{17}	4.6